Polymer Bulletin (2022) 79:2149–2171
https://doi.org/10.1007/s00289-021-03609-w

ORIGINAL PAPER

Magnesite and dolomite micro-particles: preparation, physical properties and application in bio-based polymer composite

A. Manni[1] · R. Matadi Boumbimba[2] · A. Mikdam[3] · A. El Bouari[1] · F. Addiego[4] · J. Meziani[2] · M. Wary[2]

Received: 22 June 2020 / Revised: 20 November 2020 / Accepted: 23 February 2021 /
Published online: 8 March 2021

Abstract

The study describes the potential use of dolomite $MgCa(CO_3)_2$ and magnesite $MgCO_3$ carbonates micro-particles to enhance the thermal properties of bio-based polyamide 11 (PA11). These two micro-particle fillers were first carefully analyzed in terms of composition (XRD, XRF, and FTIR), microstructure (SEM) and thermal behavior (TDA/TGA). The incorporation of these mineral fillers to PA11 by extrusion using a coupling agent conducted to an increase in thermal stability compared to the neat matrix based on TGA measurements. SEM investigations revealed that the micro-particles were well distributed and dispersed within PA11, and a good interfacial adhesion with the polymer matrix was also noted. Dolomite and magnesite were successfully used to increase the thermal stability of bio-based PA11. Nevertheless, magnesite was proved to have a higher interaction with the PA11 matrix compared to dolomite by increasing its crystallization temperature based on DSC measurements and further increasing thermal stability for a low filler content.

Keywords Dolomite · Magnesite · Polyamide 11 · Extrusion · Physical properties

✉ R. Matadi Boumbimba
rodrigue.matadi-boumbimba@univ-lorraine.fr

[1] Laboratory of Physical Chemistry of Applied Materials (LPCMA), Department of Chemistry, Faculty of Sciences Ben Msik, Hassan II University, Casablanca, Morocco

[2] Université de Lorraine, CNRS, Arts et Métiers ParisTech, LEM3, F-57000 Metz, France

[3] ENSAM Casablanca, Hassan II University of Casablanca, Avenue Hassan-II, Agadir, Morocco

[4] Department Materials Research and Technology (MRT), Luxembourg Institute of Science and Technology (LIST), ZAE Robert Steichen, 5 Rue Bommel, L-4940 Hautcharage, Luxembourg

Introduction

The Moroccan soil and subsoil contain various useful mineral substances. They are directly related to regional and local geological history. The reserves and contents of these substances are very variable. It is mainly carbonate materials made of mineral raw materials rich in magnesium oxide and calcium, including these materials, that are abundant and available at low cost. The need for temperature-resistant materials and the increasing demand from industry for natural materials have also guided this research towards the field of composites. In this context, magnesite and dolomite are one of the most desirable materials in this work because of their thermal and mechanical properties [1]. The use of magnesium oxide rich basic materials such as magnesite and dolomite in industrial applications is dependent on knowledge of their physical–chemical properties. However, research on new ways of valorization is under investigation. This study aimed to prepare bio-based polymer composites reinforced with magnesite and dolomite. Due to the advent of increasingly stringent environmental standards, many industries today are betting on the use of materials in whole or in part from renewable resources, for many applications [1–3]. These materials can be obtained, as regards the bio-sourced polymers, from vegetable oils [4, 5]. Since the physical properties of these materials are usually less interesting than those of polymer resins derived from fossil resources, their reinforcement by mineral fillers is generally considered [6]. In our study, we selected as polymer matrix a special grade of polyamide 11 (PA11) that is a bio-based polymer obtained from renewable castor seeds. This polymer will be reinforced by dolomite and magnesite fillers for the preparation of a composite with improved refractory properties. The mineral fillers of dolomite and magnesite coming from the Moroccan quarries will be first carefully characterized, before being used for the preparation of the composites by extrusion.

Materials

Dolomite and magnesite

Magnesite is magnesium carbonate of formula $MgCO_3$ and theoretical composition MgO: 47.7%; CO_2: 52.3%. It does not melt but decomposes at 1700 °C, while the residual MgO melts at 2800 °C. This magnesia is provided in three forms: (1) raw materials; (2) calcined at 850 °C; (3) grilled to death and agglomerated (bricks at 1500–1800 °C) (Ministry of Energy and Moroccan Mines). This material is used to make a special cement for the tile industry, especially for grinding wheels and abrasive coatings for grinding machines. It is sometimes called metallic cement [7]. Moreover, the dolomite $MgCa(CO_3)_2$ is an important mineral composing many sedimentary rocks, dolomitic limestone and consists in calcium magnesium carbonate. In weight percentage, the contents of CaO and MgO are 30.4% and 21.7%, respectively, which corresponds to equal molecular concentrations of CaO and MgO. Dolomite has a valuable economic perspective, because it is extensively used as

construction materials, aggregate for making of cement, and source of magnesium extraction for refractory bricks [8].

Bio-based polyamide 11

Also known as polyundecanamide, nylon 11 or Rilsan, polyamide 11 (PA 11) is a high-performance thermoplastic that is produced from a bio-based product that is castor oil. In particular, PA11 is obtained by polycondensation of 11-aminoundecanoic acid (C11 amino acid) under nitrogen at a temperature of 250 °C (see Fig. 1).

The pellets of polyamide 11 were provided by ARKEMA research center of Serquigny (France). The length of the aliphatic units –CH_2—and the arrangement of the amide groups in the chain make the polyamides having various structures influencing their properties. Indeed, the aliphatic segments of the polymer play the role of flexibilizer in the amorphous phase, which contributes to the growth of the tenacity of the material [9]. Thus, PA11 can be utilized in a wide range of application domains, such as fittings and lines of gasoline, hydraulic and pneumatic circuits in automotive, and fittings for gas distribution in oil and gas industries.

Materials processing

Raw materials

Magnesite and dolomite are local resources playing an important rule for the development of sustainable construction. The ultrabasic Beni Bousera massif in the Inner Rif (Morocco) is one of the most important massifs around the western Mediterranean that contains magnesium geomaterials useful in the construction. In this study, dolomite and magnesite were used as raw materials (Fig. 2). The geomaterials are located and taken in the Beni Bousera massif (internal Rif, Morocco), especially in Tafidest region about 103 km SW of the Tetouan city precisely between Jnan Enneich and Bouhmad, Chefchaouen province (magnesite N35° 13′11.5″ W004° 43′49.1″ and dolomite N35° 16′42.9″ W004° 51′41.82″) [1]. The raw samples extracted in the field were crushed and dried in the open air, and then steamed at 110 °C for 24 h. The dry materials were introduced into jars into which balls of various diameters were added. The crushing was performed for a duration of 30 min. The obtained powder was homogenized and then sieved to recover micro-particles using a filter enabling to extract size < 63 µm [10, 11].

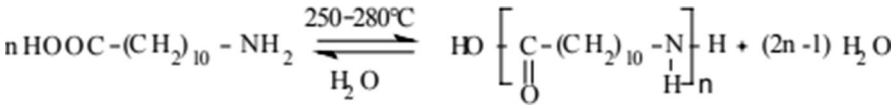

Fig. 1 Polycondensation reaction used to prepare the bio-based polyamide 11

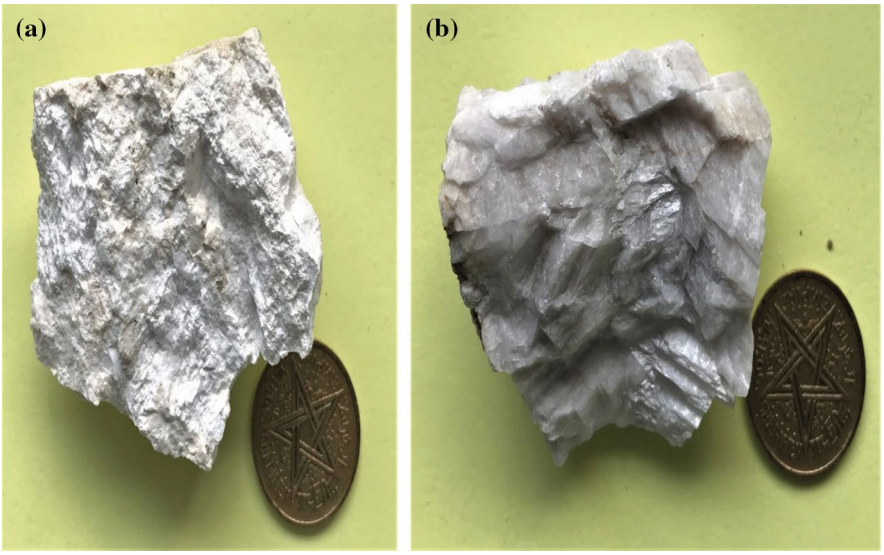

Fig. 2 **a** Macroscopic aspects of extracted dolomite and **b** magnesite samples used in this study

Silane modification of dolomite, magnesite, and melt mixing

Since polyamide 11 and natural dolomite or magnesite are not compatible due to their inherent different surface chemistry, before processing the dolomite and magnesite powder were first modified by silane as a coupling agent. The method used for this surface modification consisted of adding the liquid silane solution on an amount of dolomite or magnesite powder. After an exposure of 1 day at room temperature, the modified powder was then used for the preparation of the bio-based composites. The composite preparation was conducted by the means of melt mixing process. PA11, dolomite and magnesite were first dried overnight at 80 °C in a vacuum oven to remove moisture. The compounding was conducted with a micro-extruder DSM X'Plore 15 cc with nitrogen as purging gas. Extrusion was done at 210 °C with a residence time of 6 min. Screw speed was initially set at 100 rpm to facilitate the introduction of the materials in the extruder, then the speed was increased to 150 rpm to increase the extrusion force, and hence, the micro-particle dispersion. Three concentrations of fillers were used: 5, 10 and 15 wt%. The extruded strands were cut by means of a pelletizer into 3–5 mm length pellets. The composite characterization was conducted on these pellets.

Characterizations

The geomaterials used in this study have a wide range of properties and applications. Their market values depend on their geochemical, mineralogical and morphological properties. Structural analysis enables to determine the percentage of the

different oxides present in the geomaterial. Samples in powder form less than 63 µm in size were analyzed by X-ray fluorescence (XRF). The apparatus used is a wavelength dispersion spectrometer—Type AXIOS (UATRS). X-ray diffraction (XRD) measurements were performed on using a PANalytical X'Pert Pro diffractometer equipped with Cu X-ray radiation source (Cu $K_{\alpha}=1.5406$ Å) operating at a voltage of 45 kV and a current of 40 mA. Fourier transform infrared (FTIR) spectra were recorded with a Bruker Tensor 27 spectrometer in the range of 4000–500 cm^{-1} with 4 cm^{-1} of resolution. Thermogravimetric analyses (TGA) and differential thermal analyses (DTA) were performed with a SETARM LABSYSTM EVO 1F apparatus in air and at 5 °C/min. The observation of a coherent mineral material (e.g., rock, mineral) with a polarizing light optical microscope enables to observe in detail, by magnification up to 1000 times, its texture (shape, size and arrangement of its mineral constituents) and the optical criteria of the minerals (habitus, color, cleavage, pleochroism, relief, polarization tint, etc.) that allow the identification of each mineral species. To observe the sample under an optical microscope it is necessary that this sample is of a thickness of the order of 30 µm to be transparent. The preparation of such a thin specimen relies on cutting a cube of the sample with dimensions, $4\times2\times2$ cm, then polishing one of the large face, and sticking it onto a glass plate using a special resin (highly transparent glass and resin to be selected). Then, a grinding machine was used to reduce sample thickness in a gradual and gentle manner to avoid removing the minerals from the sample. Once, the thickness was of the order of 30 microns, the sample was covered with a special slip to protect it and make it brighter. Dolomite and magnesite morphology was studied by means of a polarized light microscope with the longitudinal polarization analysis (LPA) method. The morphology of the materials was also investigated using a scanning electron microscope (SEM) JEOL JSM-IT 100.

Concerning the bio-based composites, differential scanning calorimeter (DSC, Mettler-Toledo) testing was performed to analyze the thermal transitions of the materials. For this analysis, samples (between 5 and 10 mg) were sealed in aluminum pans. The heating and cooling rates were set to 10 °C.min^{-1}. Tests were performed under nitrogen gas purge. For all the materials, the first heating was used for eliminating the thermal history of the material. Accordingly, each sample was heated from 0 °C to 250 °C, and then cooled to 0 °C before a second heating scan up to 250 °C. The glass transition temperature (T_g) and melting temperature (T_m) were determined from this second heating scan. The crystallization temperature (T_c) was obtained from the cooling scan. T_g was determined at the mid-point of heat capacity changes, T_m was taken as the onset peak position of the endothermic, and T_c was taken as the onset peak position of the exothermic. By integration of the corresponding peaks, we have determined the different heats of crystallization and melting (ΔH_c and ΔH_m). These values (in J/g) can be corrected from a dilution effect linked to the fraction of fillers into the matrix, e.g., see Eq. 1 where *ww* is the fillers weight fraction. $\Delta H'_m$ can be calculated with the same approach [12].

$$\Delta H'_C = \frac{\Delta H_C}{1 - ww} \tag{1}$$

The degree of crystallinity (in %) was estimated with Eq. (2).

$$X_c\,(\%) = \frac{\Delta H'_m}{\Delta H_{100\%}} \times \frac{100}{1 - ww} \tag{2}$$

where $\Delta H_{100\%}$ represents the heat of melting for 100% crystalline isotropic PA11, which is taken equal to 189 J/g [13].

The TGA is the most widely used method to characterize the degradation of polymers. To this end, a Mettler-Toledo TGA 2 equipment was used with a nitrogen gas purge from 25 to 800 °C (10 °C/min). There are several parameters that are of interest, the onset temperature of the degradation that corresponds to 10% of degradation (T_{onset}), the mid-point of degradation ($T_{50\%}$), the end temperature of degradation (T_{end}), and the fraction of non-volatile residue at the highest temperature used.

Results and discussions

Characterization of raw materials

X-ray fluorescence (XRF)

The chemical analysis obtained by XRF (Table 1) showed a variable composition with the presence of several major chemical elements of magnesite and dolomite. This last ceramics generally consists of 22.73% CaO, 20.63% MgO and 51.02% fire loss due to the presence of CO_2, with the presence of traces of oxides such as Al_2O_3 (1.96%) and SiO_2 (3.06%). The mixture of CaO and MgO phases is referred as dolomite. Due to the inherent basic oxides, it has a good corrosion resistance against alkalis [14]. It is a high melting point compound with a good refractoriness [15]. Besides, the high thermodynamic stability of CaO and MgO at high temperatures makes dolomite very resistant under reducing conditions. Moreover, the chemical compositions of the magnesite (wt%) was determined by X-Ray Fluorescence (XRF) showing a high content of magnesium oxide (42.63%). Accordingly, it can be concluded that this high content in MgO can provide refractory properties because of its high melting point, its high heat shock and its excellent resistance to slag.

Table 1 Chemical composition of dolomite and magnesite in oxides (wt%)

Samples	SiO_2	Al_2O_3	Fe_2O_3	MgO	CaO	K_2O	Na_2O	P_2O_5	MnO	SO_3	TiO_2	LOI*
Dolomite	3.06	1.96	0.13	20.63	22.73	0.06	0.19	0.02	0.01	0.06	0.13	51.02
Magnesite	1.78	0.89	0.09	42.63	2.03	0.03	0.13	0.01	–	–	0.06	52.35

*Loss on ignition at 1000 °C

Structure analysis

The XRD diffractograms of the raw materials are shown in Fig. 3a, b. The main peaks of the magnesite raw samples were indexed with the reference pattern of magnesite $MgCO_3$ (JCPDS Card No. 086-2345), while the main peaks of the dolomite raw samples were indexed with the reference pattern of dolomite $MgCa(CO_3)_2$ (JCPDS Card No. 075-1761). In particular, the main peaks matched with the magnesite reference pattern exhibiting reflections at 2θ ~32.562°, 35.752°, 38.672°, 42.915°, 46.766°, 51.520°, 53.749°, 61.289°, 62.270°, 66.318°, 68.207°, 69.193°, and 70.199°, corresponding to the Bravais-Miller indices planes (104), (006), (110), (113), (202), (024), (018), (211), (122), (214), (208), (119) and (300) (Table 2). The rhombohedral crystalline structure of the raw magnesite sample was hence confirmed (Fig. 3a). As minor phases, the presence of periclase, dolomite and chlorite phases was noted in the raw magnesite samples. Concerning the raw dolomite samples, the presence of the rhombohedral dolomite with the reflections at $2\theta \sim$ 31.02°, 33.68°, 35.43°, 43.93°, 52.354°, 68.24° and 76.806° corresponding to the planes (104), (006), (015), (021), (205), (01 11) and (21 -8) was confirmed (Fig. 3b, Table 3). The presence of goethite and periclase as minor phases was also detected in the dolomite raw specimen. The average crystallite size based on the Scherrer's equation is found to be 31.63 nm for magnesite and 44.54 nm for dolomite (Tables 2 and 3).

Chemical bonds analysis

The FTIR analysis technique allows us to detect the presence of silane molecules at the surface of the carbonates, based on the comparison of the different absorption bands of the functional groups present for the carbonates before and after their surface modification. We give the IR spectra of the raw magnesite and magnesite modified by the silane. The IR spectra of the raw dolomite and the modified dolomite are provided too. For the two materials, the IR spectrum exhibits the presence of bands at 3572 cm^{-1}, 3611 cm^{-1}, 3642 cm^{-1}, and 3672 cm^{-1} expressing the existence of vibration modes, mainly attributed to the O–H functional groups [1, 16, 17] (Fig. 4a, b). On the other hand, the observed bands at 1659 cm^{-1} and 1743 cm^{-1} could be associated to the bending vibration of the –OH group. Besides, the characteristic bands at 2536 cm^{-1}, 1506 cm^{-1}, 1450 cm^{-1}, 883 cm^{-1} and 725 cm^{-1} are attributed to stretching-bending, asymmetric stretching, out of plane bending, and in plane bending of CO_3^{2-} group in both materials, respectively. Other peaks were detected at 538 cm^{-1}, 539 cm^{-1} and 598 cm^{-1} [1, 16]. The low bands at 640 cm^{-1}, 665 cm^{-1}, and 990 cm^{-1} from Si–O–Mg vibration observed for the two samples indicate the presence of sepiolite [11, 16, 18]. More importantly, the appearance of an intense band at 1017 cm^{-1} after silane treatment may be due to an interaction between the absorbed silane and the material surface. In particular, this new band can be due to the formation of hydrogen bonds between the carbonyl groups of the magnesite and the dolomite and the hydrogen atoms of the silane [19]. Note that this absorption of silane also conducted to a shift of various bands as reported in Table 4, highlighting a change of chemical environment.

Fig. 3 **a** X-ray diffraction (XRD) analysis of the raw magnesite specimen. **b** X-ray diffraction (XRD) ▶ analysis of the raw dolomite specimen

Thermal analysis

The TGA-DTA curves of the dolomite recorded from room temperature to 1200 °C are shown in Fig. 5a. The dolomite exhibited four endothermic peaks. The first endothermic peak at about 96 °C and the second at about 325 °C can be assigned to the removal of moisture and structural water from the powder, respectively. It is to be noted that the elimination of moisture/water does not modify the crystalline structure of the dolomite with a mass loss of 4%. The endothermic peak ranging between 550 and 670 °C may be due to the successive decomposition of the calcium carbonate (calcite) and the magnesium carbonate (magnesite) with the release of CO_2 (mass loss of 4%).The last exothermic peak observed at about 1100 °C corresponds to the structural reorganization of the periclase (MgO). Figure 5b shows the TGA-DTA curves of magnesite from room temperature to 1200 °C. In particular, the main peak positioned at 600 °C is due to the decomposition of the carbonate accompanied by a loss of mass of about 36%. Last, a weak peak noted at about 850 °C can be attributed to the transformation of magnesite into periclase with a loss of mass of 2%. The same shift in decomposition temperature between two carbonate types was reported by Kumar and coworkers [1, 20–23].

Morphological characterization

The SEM observation of the two carbonate powders reveals several interesting points. Different powder sizes were analyzed (granular fraction of 100 µm, 50 µm and 10 µm) in the case of magnesite and dolomite (Figs. 6, 7, 8, 9). In the case of the magnesite powder with a granular fraction of 10 µm, the presence of very fine particles in the form of a powder of homogeneous appearance was noted. It was hypothesized that this fine powder is highly rich in magnesium oxide (Fig. 6a). At the level of the heterometric, there was a poor ranking on the different scales of the granular fraction of 10 µm, which is probably due to the non-optimal grinding method (Fig. 7). The overall appearance of the surface of this sample was porous and was not homogeneous with granular fractions of 50 µm (Fig. 6b). The granular fraction of 100 µm (Fig. 6c) showed different sizes, the first grains having large sizes were rounded with slightly blunted edges and angles.

Figure 9 shows the SEM micrographs recorded for dolomite powder in which the results reveal a clearer and more apparent automorphic crystalline form. The rhombohedral aspect structure of the crystals of dolomite was clearly observed with sharper edges (case granular fraction of 100 µm). Microporosities were also observed, appearing on the images as dark gray areas in different fractions of 10 µm, 50 µm and 100 µm (Fig. 8a–c). At the texture level, there is a homogeneous color, indicating that the dolomite matrix shows a higher calcium and magnesium content in the gray areas. Besides, we can observe that the 10 µm granular fractions of dolomite have very fine grains with important compactness (Fig. 8a).

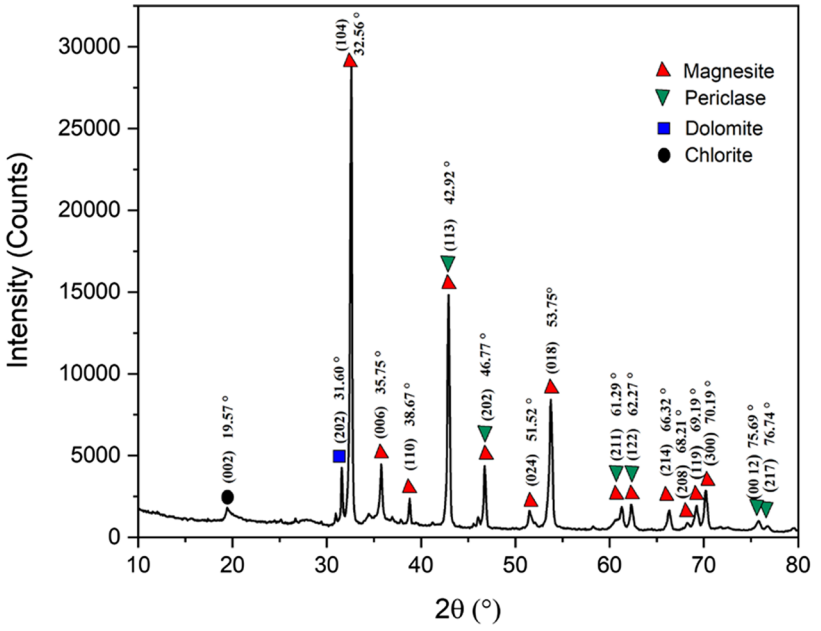

(a) X-ray Diffraction (XRD) analysis of the raw magnesite specimen

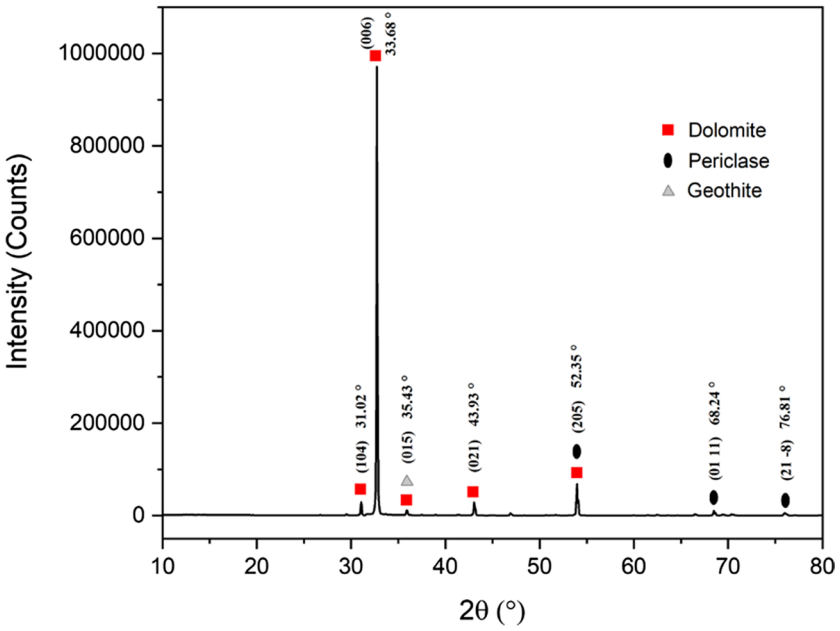

(b) X-ray Diffraction (XRD) analysis of the raw dolomite specimen

Table 2 Magnesite phase analysis in magnesite raw samples by XRD

Magnesite raw material						
Average crystallite size (nm) = 31.63						
N Peak	Peak position (2 Theta)	FWHM	(hkl)			Crystallinity (nm)
1	19.57	0.23222	0	0	2	34.72
2	31.60	0.23222	2	0	2	35.55
3	32.56	0.23222	1	0	4	35.64
4	35.75	0.23222	0	0	6	35.95
5	38.67	0.23222	1	1	0	36.26
6	42.92	0.23222	1	1	3	36.76
7	46.77	0.23222	2	0	2	37.27
8	51.52	0.23222	0	2	4	37.99
9	53.75	0.29028	0	1	8	30.68
10	61.29	0.29028	2	1	1	31.81
11	62.27	0.34834	1	2	2	26.64
12	66.32	0.34834	2	1	4	27.24
13	68.21	0.29028	2	0	8	33.05
14	69.19	0.34834	1	1	9	27.70
15	70.19	0.40639	3	0	0	23.89
16	75.69	0.46445	0	0	12	21.66
17	76.74	0.40639	2	1	7	24.93

Table 3 Dolomite phase analysis in dolomite raw samples by XRD

Dolomite raw material						
Average crystallite size (nm) = 44.54						
N Peak	Peak position (2 Theta)	FWHM	(hkl)			Crystallinity (nm)
1	31.02	0.17417	1	0	4	47.34
2	33.68	0.17417	0	0	6	47.66
3	35.43	0.17417	0	1	5	47.88
4	43.93	0.17417	0	2	1	49.18
5	52.35	0.17417	2	0	5	50.82
6	68.24	0.29028	0	1	11	33.06
7	76.81	0.2832	2	1	-8	35.80

The observations performed on the thin sections of dolomite (D) showed a heterogeneous texture composed of finely graded masses of dolomite cut by veinlets filled with secondary alteration products (Fig. 10).

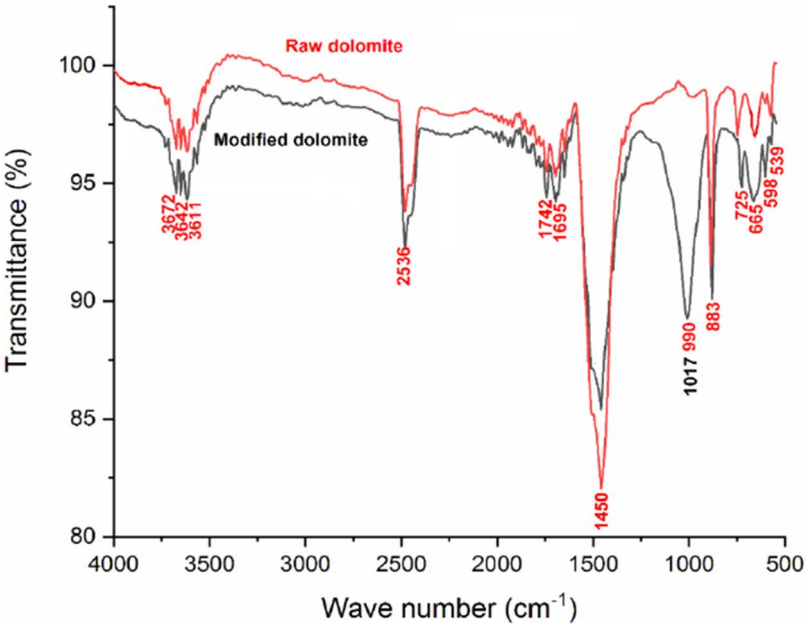

(a) FTIR spectrum of the dolomite

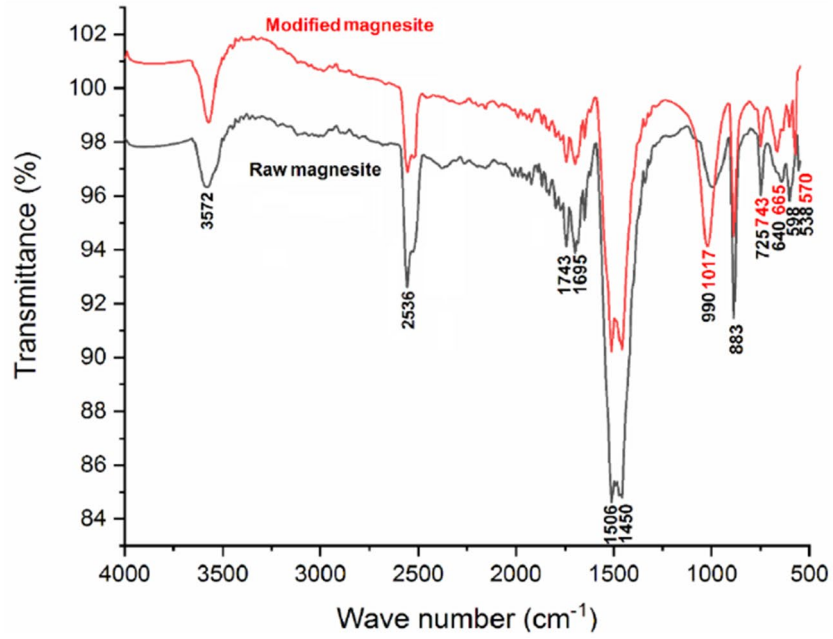

(b) FTIR spectrum of the magnesite

Fig. 4 **a** FTIR spectrum of the dolomite. **b** FTIR spectrum of the magnesite

Table 4 IR bands of raw magnesite before and after silane modification

Bands before modification (cm^{-1})	Bands after modification (cm^{-1})
538	570
640	665
725	743
990	1017

Micrographs A and B taken in natural light (LN) and polarized light (LP), respectively, showed the finely grated mass of dolomite recognizable on micrograph B by its high polarization tints (of the 3rd and 4th order on the Newton chromatic scale). The high magnification (micrograph D) revealed that the late veinlets, which cross the dolomite mass, were composed mainly of chlorite and incidentally periclase, quartz and some opaque grains (iron oxides as goethite).

The observations conducted on the thin sections of magnesite (M) showed a granoblastic texture with millimeter-sized joined grains of magnesite (Fig. 11). The dolomite was recognizable on both micrographs A and B, taken in natural and polarized light, respectively, by its almost orthogonal double cleavage and its high polarization shades with pink and green iridescence. At high magnification (micrographs C and D), the magnesite grains contain some secondary minerals in the form of small muscovite/chlorite flakes as well as some calcite, periclase and rare opaque grains with a reddish sheen (hematite or goethite).

To conclude, the polarizing optical microscope observations show that the samples used in this study are actually composed of well-expressed crystals of dolomite and magnesite, which corresponded almost to the entire mass of the samples. In addition to dolomite and magnesite, the samples contain very small quantities of secondary minerals (less than 5%) of chlorite, periclase, calcite, quartz, iron oxides, etc. These secondary minerals appear from late formation and from secondary alteration processes. It should be noted that the mineralogical compositions of the two samples D and M, revealed by optical microscope observations, corroborate the results of the X-ray diffraction.

Bio-based composite morphology

The morphology of composites of different compositions was evaluated by SEM as represented in Figs. 12 and 13. The dolomite and magnesite particles exhibited a spherical shape. At the same time, there was no macrodefect such as crack. These features are important for ensuring a high processing quality in the case of ceramic-filled composites. Indeed, a high surface quality of the substrate is important for the effectiveness of the insulation.

As reported in Figs. 12, 13 and 14, both dolomite and magnesite particles were homogeneously distributed and well dispersed within the polyamide matrix. This good dispersion is mainly due to the use of silane modification, which increases the adhesion between particles and polymer matrix [24]. In both cases, the particles

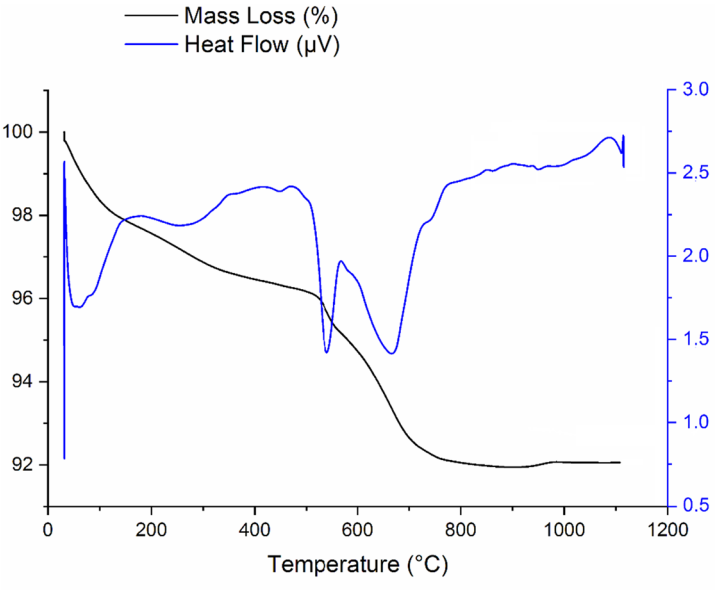

(a) TGA and DTA curves for dolomite mineral

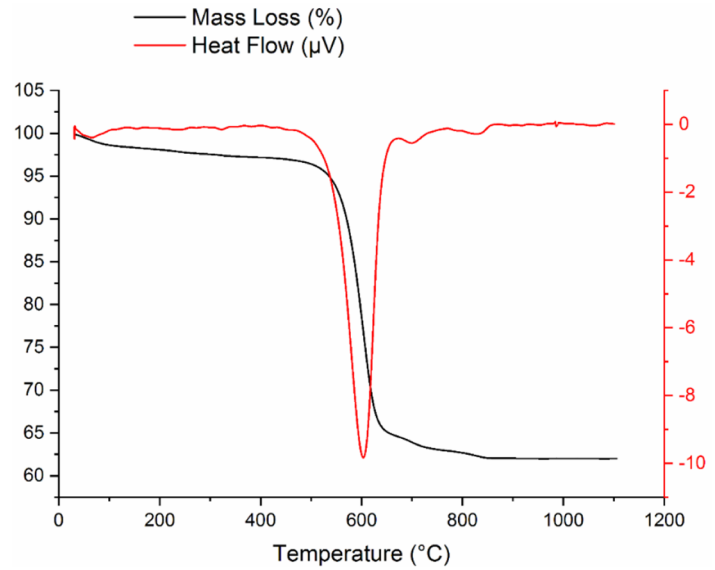

(b) TGA and DTA curves for magnesite mineral

Fig. 5 **a** TGA and DTA curves for dolomite mineral. **b** TGA and DTA curves for magnesite mineral

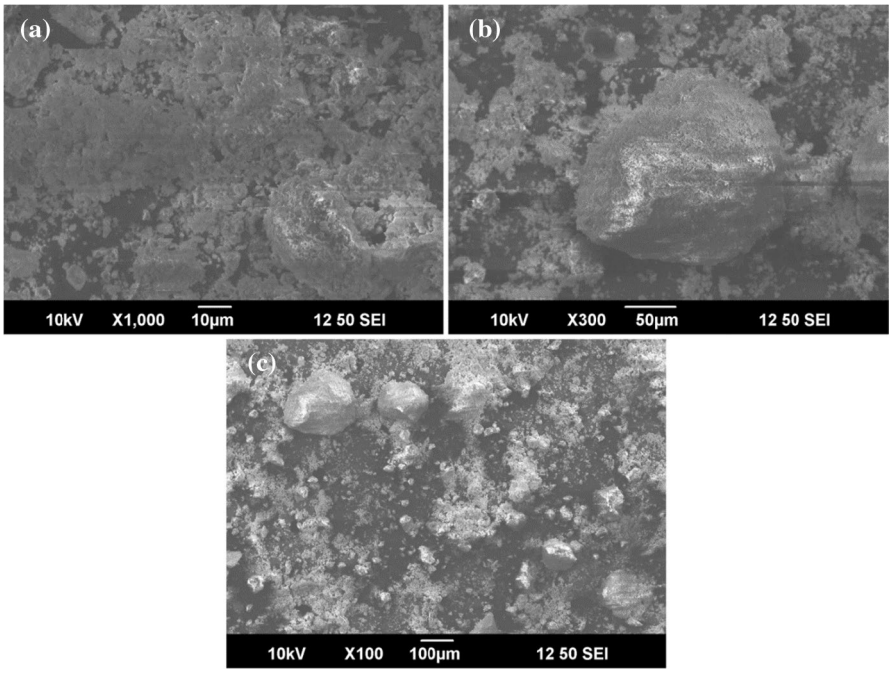

Fig. 6 SEM images of raw magnesite powder. Fraction of **a** 10 µm, **b** 50 µm, and **c** 100 µm

exhibited a spherical shape, and a good interaction with the PA11 matrix, as no interfacial debonding appeared on the SEM images. At high magnification, the interfacial adhesion seemed good even if in some places small ceramic particles were pullout.

As reported in several works focused on polymer reinforced with particles, the good dispersion and good interfacial adhesion can lead to increased physical properties. In this paper, the TGA and DSC analyses were performed on pristine PA11 and PA11 filled with different amounts of dolomite and magnesite.

Bio-based composite thermal properties

Figure 15 and Tables 5 and 6 depict the DSC analysis in terms of T_g, T_m, T_c and crystallinity. As observed, the addition of dolomite or magnesite does not lead to a change in the melting temperature. It can be also observed in the case of PA11

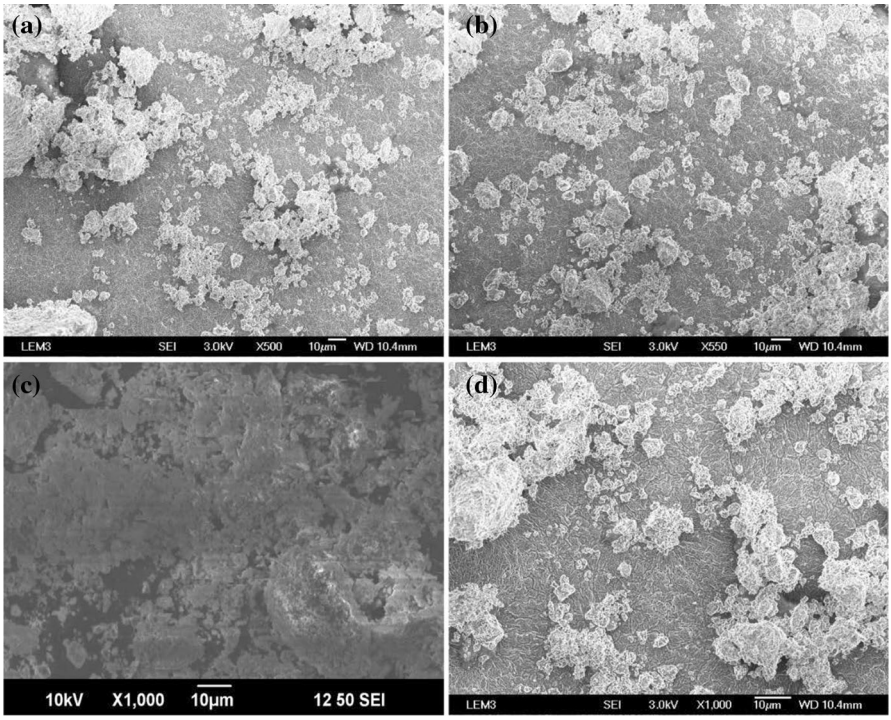

Fig. 7 SEM images of the raw magnesite powder at different scales of the 10 µm granular fraction

filled with dolomite that the crystallization temperature was unchanged whatever the dolomite concentration. However, this crystallization temperature increased with the addition of magnesite compared to pure PA11. This means that PA11 interact with magnesite maybe through a nucleating effect of the ceramic for the polymer crystallization. Consequently magnesite may play an important rule to enhance the thermal and mechanical properties of PA11. However, only a weak increase in crystallinity is noted when adding 5 wt% of magnesite compared to neat PA11, for the other concentration crystallinity is quite unchanged. This result may be due to the possible physical hindering of PA11 by magnesite micro-particles during crystallization, this mechanisms being not active for a magnesite concentration of 5 wt%.

From the TGA results (Fig. 16), it can be observed that the addition of dolomite and magnesite had a small but significant effect on the thermal stability of the

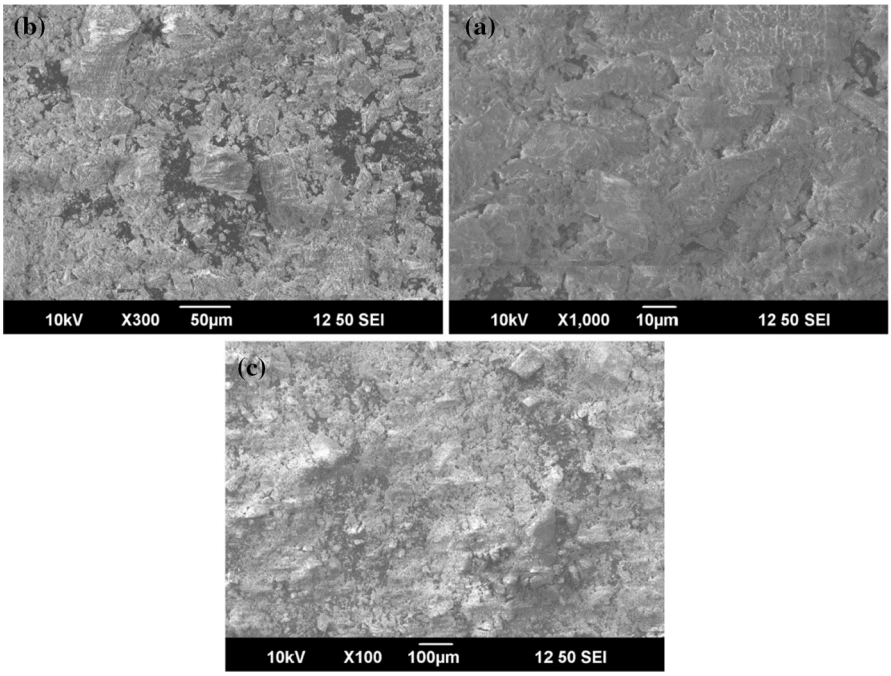

Fig. 8 SEM images of raw dolomite powder. Fraction of **a** 10 µm, **b** 50 µm, and **c** 100 µm

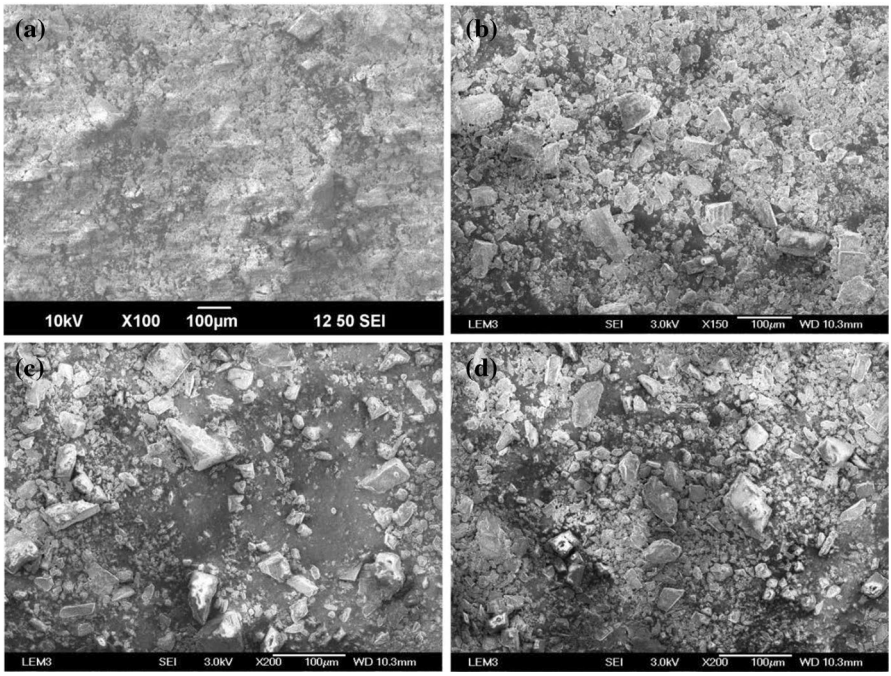

Fig. 9 SEM images of crude dolomite powder at different scales of the 100 µm granular fraction

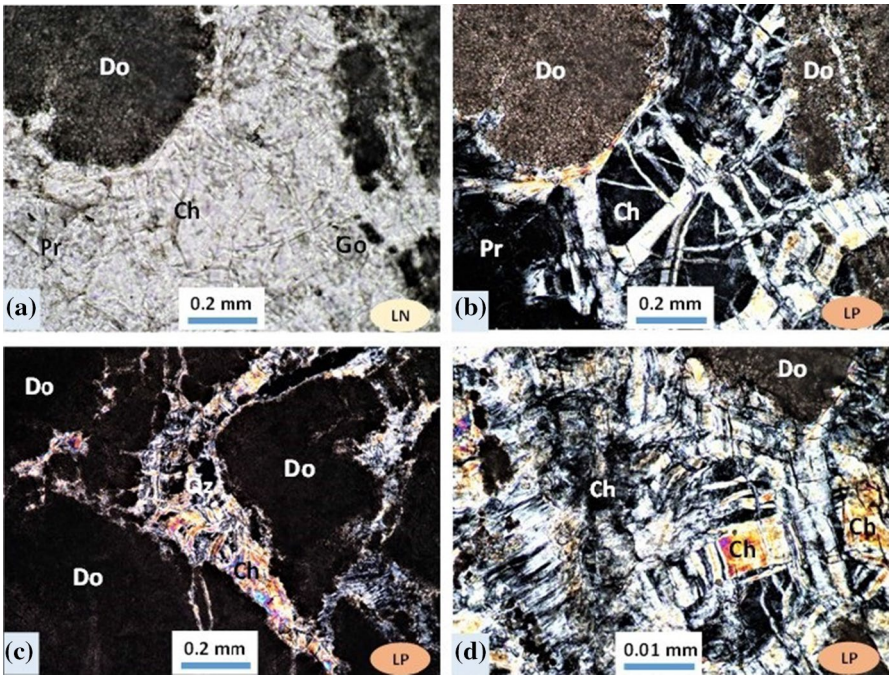

Fig. 10 Micrographs of the thin dolomite section (D). *LN* natural light, *LP* polarized light—*Do* dolomite, *Ch* chlorite, *Go* goethite, *Pr* periclase, *Qz* quartz

composites. The onset decomposition temperature (T_{onset}), and the mid-point of degradation ($T_{50\%}$) exhibited a maximum increase of about 5 and 10 °C, respectively, for both tested composites compared to the pristine PA11. The increase in thermal stability increased gradually when increasing the filler fraction the case of the dolomite particles, while the thermal stability was quite similar whatever the fraction of magnesite filler. This finding confirms a higher matrix–filler interaction in the case of magnesite compared to dolomite, confirming DSC results. This slight increase in the decomposition temperatures maybe due to the ability of magnesite or dolomite fillers to obstruct volatile gas produced by thermal decomposition [25]. Some works in the literature report similar observations. Furthermore, the good interfacial adhesion between dolomite or magnesite and the PA11 matrix can also explain the increase in the thermal stability by facilitating the phonon transport between the matrix and the filler. This good interfacial adhesion was explained by the use of silane to improve the filler dispersion and interaction with the polymer matrix. This result was also

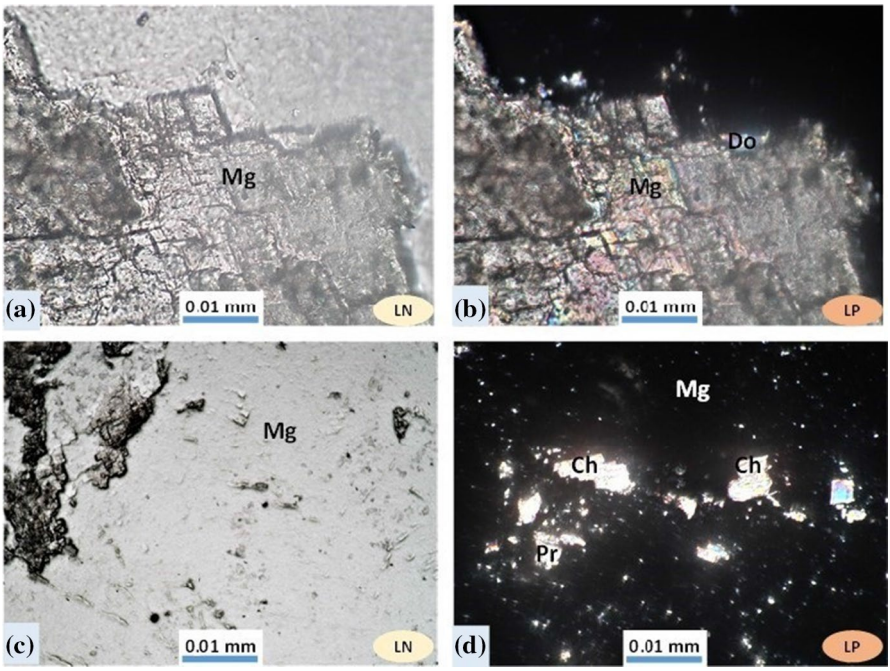

Fig. 11 Micrographs of the thin section of magnesite (M). *LN* natural light, *LP* polarized light—*Mg* magnesite, *Ch* chlorite, *Do* dolomite, *Pr* periclase

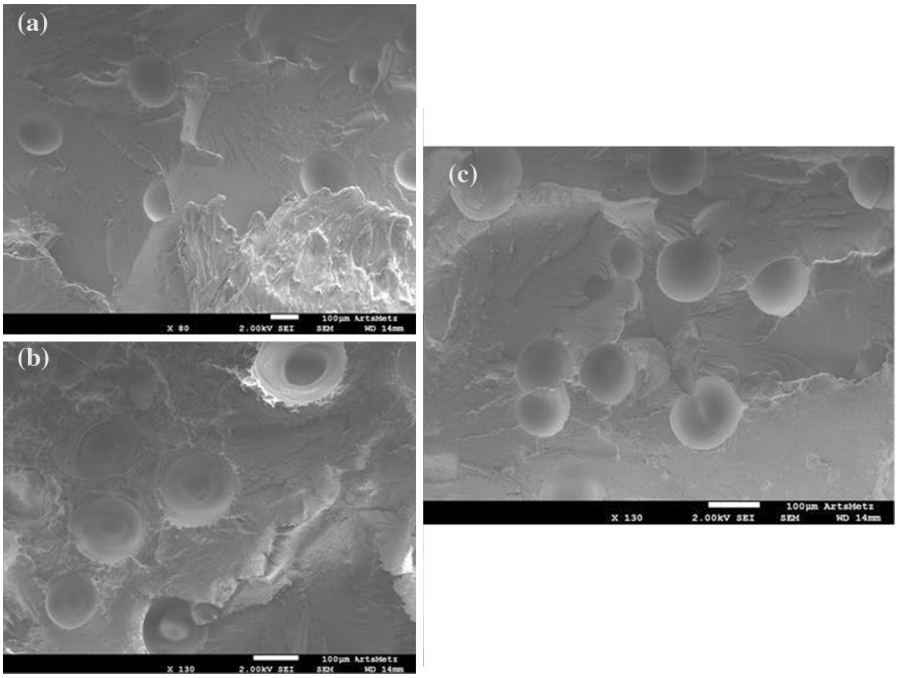

Fig. 12 SEM pictures of polyamide 11 filled with **a** 5 wt%, **b** 10 wt%, and **c** 15 wt% of modified dolomite particles

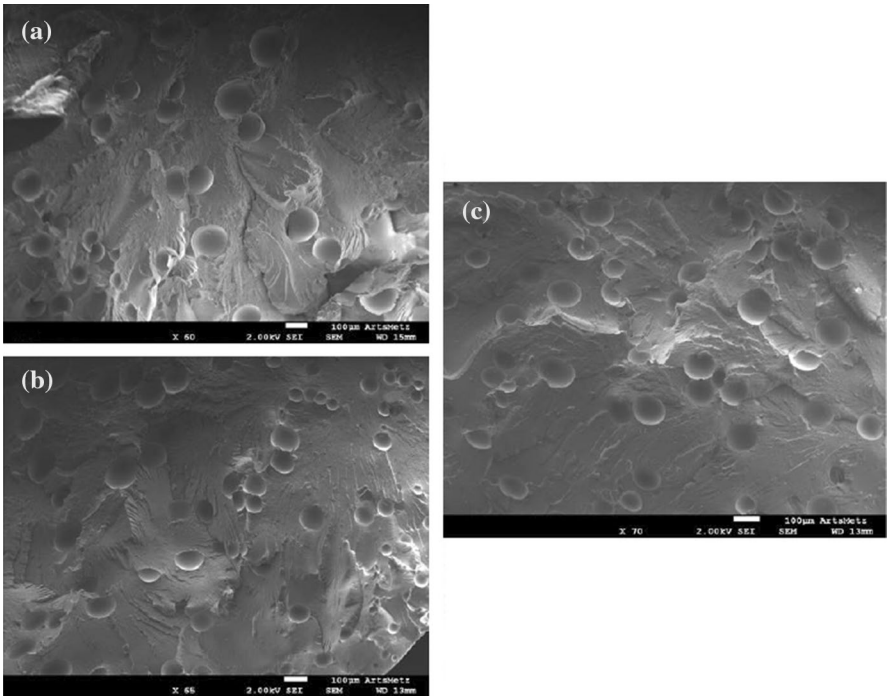

Fig. 13 SEM pictures of polyamide 11 filled with **a** 5 w%, **b** 10 wt%, and **c** 15 wt% of modified magnesite particles

reported by Vyazovkin [26], who studied the thermal stability of PLC/SiO_2 nanocomposites. The author explains the enhancement of thermal stability by the fact that SiO_2 nanoparticles have a lot of surface silanoil groups acting as initiator for ring opening polymerization of ε-caprolactone, enhancing the interaction with the polymer matrix [27, 28].

Conclusions

The study describes the influence of carbonates micro-particles on the morphological and thermal properties of bio-based polyamide 11 (PA11) composites, using numerous analytical techniques (XRD, XRF, DTA-TGA, DSC, FTIR, SEM) to characterize the raw materials (magnesite, dolomite) and bio-based polyamide composites.

After powdering and characterizing the raw magnesite and dolomite powders, bio-based polyamide composites, were prepared by the melt mixing of PA11 with magnesite or dolomite fillers. Note that prior to extrusion, the ceramic powders were treated with silane. SEM observations of the obtained materials have shown that both magnesite and dolomite particles were well distributed and dispersed within the PA11 matrix, and presented a spherical shape. It was also observed that the filler and

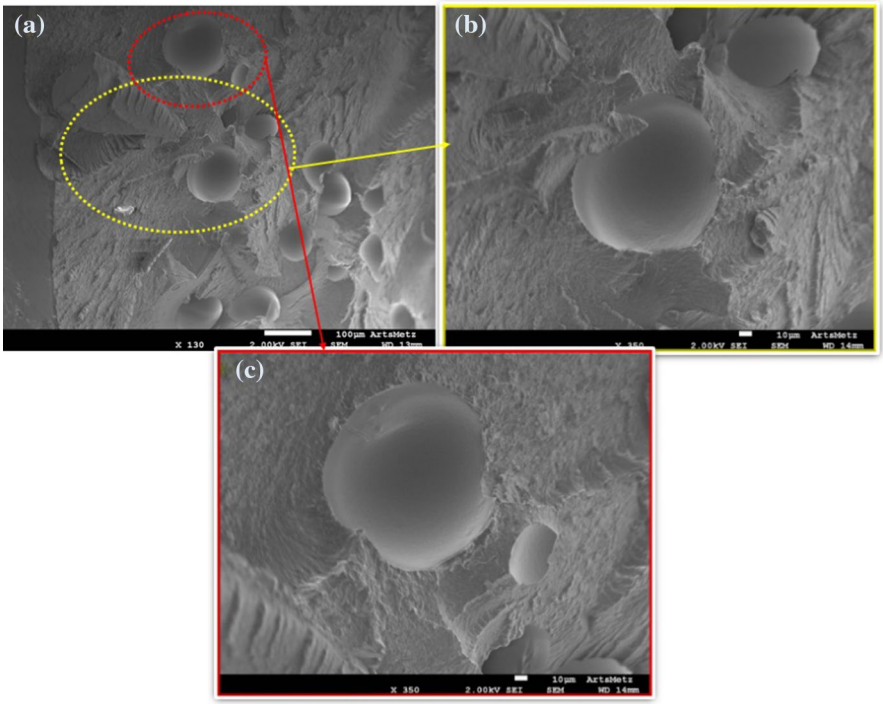

Fig. 14 High-magnification SEM pictures of polyamide 11 filled with 5 wt% of modified magnesite particles

matrix interfacial adhesion was good, which was expected to play an important rule on the thermal properties. According to DSC results, the addition of dolomite filler did not influence the melting nor crystallization process of PA11. However, in the case of magnesite particles, the crystallization temperature of PA11 was increased in the presence of magnetite, indicating a potential matrix–filler interaction. This interaction may be due to a crystallization nucleating effect of magnesite. TGA analyses performed on the composites showed a significant increase in all the onset temperatures, revealing that both magnesite and dolomite micro-fillers enhance the thermal stability of PA11. This increase in thermal stability appeared more efficient in the case of magnesite compared to dolomite.

Our future works will deal with a further improvement of the dispersion state of these ceramic particles reaching a sub-micron size and studying the viscoelastic and tensile behavior of the resulting composites.

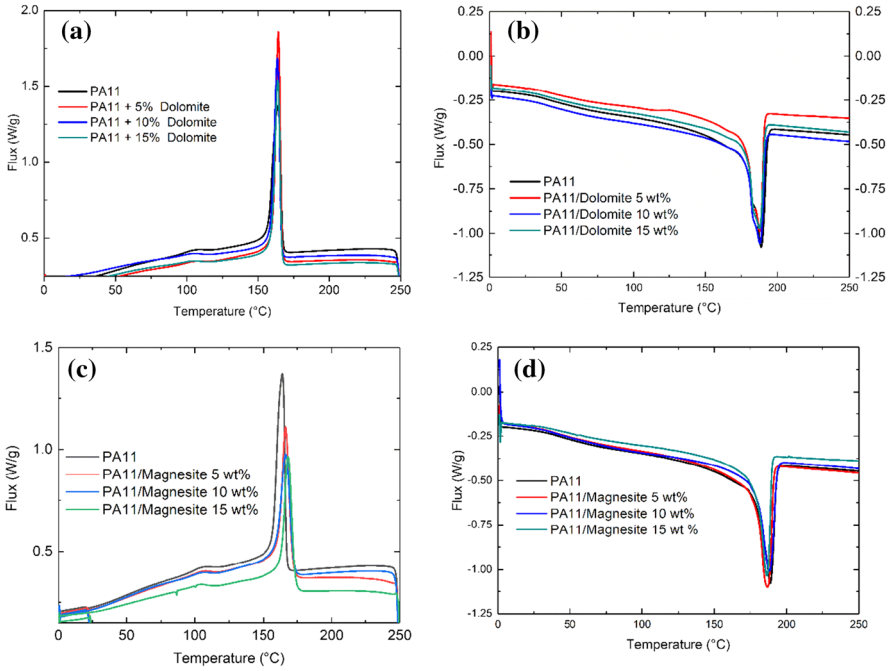

Fig. 15 DSC thermal curves of pristine PA11 and its composites for different amounts of fillers

Table 5 DSC results for PA11/dolomite composites

Sample	T_g (°C)	T_c (°C)	$\Delta H'_c$ (J.g^{-1})	T_m (°C)	$\Delta H'_m$ (J.g^{-1})	X_c (%)
PA11	41.6	164.2	28.1	189.5	35.2	21.7
PA11/D-5%	42.2	164.4	24.8	188.0	34.1	22.2
PA11/D-10%	43.8	163.7	26.1	188.4	34.6	23.7
PA11/D-15%	41.7	164.1	23.1	188.0	29.4	21.3

Table 6 DSC results for PA11/magnesite composites

Sample	T_g (°C)	T_c (°C)	$\Delta H'_c$ (J.g^{-1})	T_m (°C)	$\Delta H'_m$ (J.g^{-1})	X_c (%)
PA11	41.6	164.2	28.1	189.1	35.2	21.7
PA11/M-5%	42.4	166.3	25.1	188.0	36.7	23.8
PA11/M-10%	44.6	166.3	25.4	188.4	32.7	22.4
PA11/M-15%	43.5	168.4	21.2	188.0	28.5	20.7

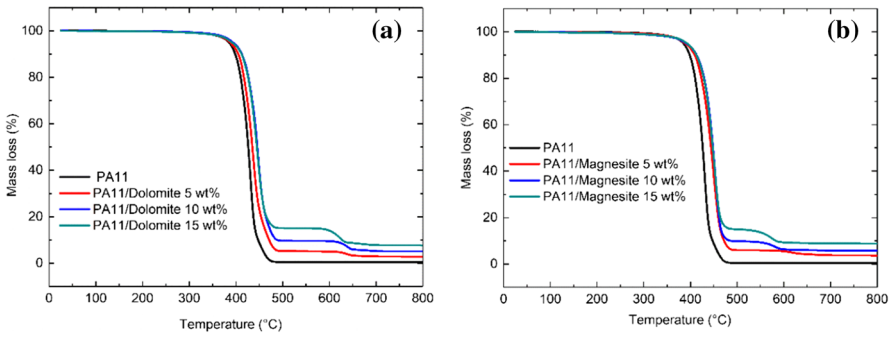

Fig. 16 TGA curves for the pristine PA11 and its composites in the case of **a** dolomite fillers and **b** magnesite fillers

References

1. Sadik C, Manni A, El Kalakhi S, El Hassani I-EEA (2019) Preparation and characterization of possible basic ceramics from Moroccan magnesite. J Aust Ceram Soc 55:415–423. https://doi.org/10.1007/s41779-018-0249-5
2. Matadi R, Hablot E, Wang K, Bahlouli N, Ahzi S, Avérous L (2011) High strain rate behaviour of renewable biocomposites based on dimer fatty acid polyamides and cellulose fibres. Compos Sci Technol 71:674–682. https://doi.org/10.1016/j.compscitech.2011.01.010
3. Nayak PL (2000) Natural oil-based polymers: opportunities and challenges. J Macromol Sci Part C Polym Rev 40:1–21. https://doi.org/10.1081/MC-100100576
4. Fan X-D, Deng Y, Waterhouse J, Pfromm P (1998) Synthesis and characterization of polyamide resins from soy-based dimer acids and different amides. J Appl Polym Sci 68:305
5. Reulier M, Avérous L (2015) Elaboration, morphology and properties of renewable thermoplastics blends, based on polyamide and polyurethane synthesized from dimer fatty acids. Eur Polymer J 67:418–427. https://doi.org/10.1016/j.eurpolymj.2014.11.036
6. Reulier M, Boumbimba RM, Rasselet D, Avérous L (2016) Renewable thermoplastic multiphase systems from dimer fatty acids, with mineral microfillers. J Appl Polym. Sci 133:n/a-n/a. https://doi.org/10.1002/app.43055
7. Sadik C, Moudden O, El Bouari A, El Amrani I-E (2016) Review on the elaboration and characterization of ceramics refractories based on magnesite and dolomite. J Asian Ceram Soc 4:219–233. https://doi.org/10.1016/j.jascer.2016.06.006
8. Aşkın A, Tatar İ, Kılınç Ş, Tezel Ö (2017) The utilization of waste magnesite in the production of the cordierite ceramic. Energy Procedia 107:137–143. https://doi.org/10.1016/j.egypro.2016.12.151
9. Thokala N, Kealey C, Kennedy J, Brady DB, Farrell JB (2017) Characterisation of polyamide 11/copper antimicrobial composites for medical device applications. Mater Sci Eng, C 78:1179–1186. https://doi.org/10.1016/j.msec.2017.03.149
10. El Haddar A, Manni A, Azdimousa A, El Amrani El Hassani I-E, Bellil A, Sadik C, Fagel N, El Ouahabi M (2019) Elaboration of a high mechanical performance refractory from halloysite and recycled alumina. Bol Soc Esp Cerám Vidr. https://doi.org/10.1016/j.bsecv.2019.08.002
11. Manni A, El Haddar A, El Amrani El I-E, Hassani AE, Bouari CS (2019) Valorization of coffee waste with Moroccan clay to produce a porous red ceramics (class BIII). Bol Soc Esp Cerám Vidr 58:211–220. https://doi.org/10.1016/j.bsecv.2019.03.001
12. Hablot E, Donnio B, Bouquey M, Avérous L (2010) Dimer acid-based thermoplastic bio-polyamides: reaction kinetics, properties and structure. Polymer 51:5895–5902. https://doi.org/10.1016/j.polymer.2010.10.026
13. Ruehle DA, Perbix C, Castañeda M, Dorgan JR, Mittal V, Halley P, Martin D (2013) Blends of biorenewable polyamide-11 and polyamide-6,10. Polymer 54:6961–6970. https://doi.org/10.1016/j.polymer.2013.10.013

14. Thomaidis E, Kostakis G (2015) Synthesis of cordieritic materials using raw kaolin, bauxite, serpentinite/olivinite and magnesite. Ceram Int 41:9701–9707. https://doi.org/10.1016/j.ceramint.2015.04.039
15. Schacht CA (2004) Refractories handbook. CRC Press, Boca Raton
16. Hajjaji M (2014) Mineralogia e transformação térmica dos materiais argilosos da região de Marrakech. Marrocos 6:75
17. Gawande MB, Branco PS, Parghi K, Shrikhande JJ, Pandey RK, Ghumman CAA, Bundaleski N, Teodoro OMND, Jayaram RV (2011) Synthesis and characterization of versatile MgO–ZrO_2 mixed metal oxide nanoparticles and their applications. Catal Sci Technol 1:1653. https://doi.org/10.1039/c1cy00259g
18. Farmer VC, Palmieri F (1975) The characterization of soil minerals by infrared spectroscopy. In: Gieseking JE (ed) Soil components. Springer, Berlin, pp 573–670. https://doi.org/10.1007/978-3-642-65917-1_17
19. Riccio M, Montanari T, Castellano M, Turturro A, Negroni FM, Busca G (2007) An IR study of the chemistry of triethoxysilane at the surface of metal oxides. Colloids Surf, A 294:181–190. https://doi.org/10.1016/j.colsurfa.2006.08.010
20. Tian L, Tahmasebi A, Yu J (2014) An experimental study on thermal decomposition behavior of magnesite. J Therm Anal Calorim 118:1577–1584. https://doi.org/10.1007/s10973-014-4068-9
21. Kıpçak İ, Isıyel TG (2015) Magnesite tailing as low-cost adsorbent for the removal of copper(II) ions from aqueous solution. Korean J Chem Eng 32:1634–1641. https://doi.org/10.1007/s11814-014-0377-8
22. Achiou B, Elomari H, Ouammou M, Albizane A, Bennazha J, Younssi SA, Amrani IEE, Aaddane A (2016) Elaboration and characterization of flat ceramic microfiltration membrane made from natural Moroccan pozzolan (Central Middle Atlas). J Mater Environ Sci 7(1):196–204
23. Kumar P, Burhanuddin A, Kumar A, Ghosh S, Sinhamahapatra HS (2015) Tripathi, Effect of titania on the microstructure evolution of sintered magnesite in correlation with its properties. Ceram Int 41:9003–9008. https://doi.org/10.1016/j.ceramint.2015.03.236
24. Dehas W, Guessoum M, Douibi A (2017) Elaboration et caractérisation d'un matériau composite à matrice polyester insaturé renforcée par la vermiculite, p 3
25. Sheila D (1993) Thermal analysis studies on the decomposition of magnesite. Int J Miner Process 37:73–88. https://doi.org/10.1016/0301-7516(93)90006-V
26. Hablot E, Matadi R, Ahzi S, Avérous L (2010) Renewable biocomposites of dimer fatty acid-based polyamides with cellulose fibres: thermal, physical and mechanical properties. Compos Sci Technol 70:504–509. https://doi.org/10.1016/j.compscitech.2009.12.001
27. Kim Y-J, Ha S-W, Jeon S-M, Yoo DW, Chun S-H, Sohn B-H, Lee J-K (2010) Fabrication of Triacetyl cellulose−SiO_2 Nanocomposites by Surface Modification of Silica Nanoparticles. Langmuir 26:7555–7560. https://doi.org/10.1021/la904362x
28. Mallakpour S, Naghdi M (2018) Polymer/SiO_2 nanocomposites: Production and applications. Prog Mater Sci 97:409–447. https://doi.org/10.1016/j.pmatsci.2018.04.002